I S A V

Journal of Theoretical and Applied Vibration and Acoustics

journal homepage: http://tava.isav.ir

A novel modeling of energy extraction from nonlinear vortex-induced vibrations

Sima Sobhanirad[a], Aref Afsharfard[b*]

[a]*Ph.D. Candidate, Department of Mechanical Engineering Ferdowsi University of Mashhad, Mashhad, Iran*

[b]*Associate Professor, Department of Mechanical Engineering Ferdowsi University of Mashhad, Mashhad, Iran*

ARTICLE INFO

Article history:
Received 31 December 2019

Received in revised form
8 April 2020

Accepted 23 May 2020

Available online 12 July 2020

Keywords:
Vortex-Induced Vibrations,

Piezoelectric Energy Harvesting,

Wake-Oscillator Model,

Fluid-Structure Interaction .

ABSTRACT

In this study, energy harvesting from two-dimensional vortex-induced vibrations of a circular cylinder is investigated. To do so, the vibratory behavior of the flexibly mounted circular cylinders is described using the nonlinear wake-oscillator model. Then, the effect of changing the flow velocity on the dynamic behavior of the cylinder is numerically obtained and validated by experimental results. The effect of changing the main parameters of the system on its electrical and vibratory behavior is investigated by employing the nonlinear electromechanical equations of motion. Unlike most previous studies that only tend to maximize the harvested energy, structural failure due to large deformation is considered in this study. For this reason, the so-called Perfection Rate (PR) parameter is introduced. By using this parameter, the application of the energy harvester is characterized, in which the energy harvesting system works efficiently, regarding its vibration amplitude, which should be small enough.

Furthermore, the proper load resistance range for the VIV-based energy harvesting system in the post-synchronization regime is obtained and it is demonstrated that the energy harvesting system with a small electromechanical coupling coefficient can effectively work in this regime.

1.Introduction

Nowadays, many studies have been done on the case of generating electrical energy from ambient vibration-based energy sources [1-3]. In this area of research, electromagnetic [4], electrostatic [5], and piezoelectric [6-8] devices are widely utilized as energy harvesters. Among these systems, piezoelectric devices can be used in a vast range of frequencies. Therefore, they

* Corresponding Author:
E-mail address: Afsharfard@um.ac.ir.(A. Afsharfard)

http://dx.doi.org//10.22064/tava.2021.102793.1125

can be good options for vibration-based energy harvesting systems [9]. One of the accessible vibration sources for energy harvesting is vortex-induced vibrations (VIV), which is studied by many researchers over the past years [10]. Generally, the VIV is described using one degree of freedom mass-spring system, in which a bluff body is oscillating in the transverse direction of fluid flow [11-15]. Facchinetti *et al.* compared three coupling models with experimental results and concluded that the acceleration coupling could predict the experimental results better than other couplings [14]. Using two coupled van der Pol equations, Farshidianfar and Zanganeh presented a model with good agreement with the empirical results in both low and high mass-damping ratios [15]. In several studies, models with two degrees of freedom have been presented to accurately predict the VIV in transverse and in-line directions [16-18].

In recent years, flow-induced vibration-based energy harvesting are studied by many researchers. Oscillations of an airfoil [19], a circular cylinder [20], and non-circular cross-section geometries such as square section bluff bodies [21], flexible membrane in fluid flow [22], PVDF piezoelectric polymer in water flow [23], cantilevered piezoelectric energy harvesters [24], flexible ceramic cylinders [25] are some of the studies concerning this field.

The vortex-induced vibrations have large amplitudes over the wide range of lock-in phenomena. This wide frequency range is proper for extracting energy. On the other hand, piezoelectric harvesters are proper for harvesting energy from fluid flow oscillations because they have a simple structure and can easily be excited to the VIV. Also, comparing to other energy harvesting methods, piezoelectric materials have a larger power density [26].

In the present study, a two-dimensional system is equipped with a piezoelectric device. Coupled electromechanical equations are obtained to describe the vibratory and electrical behavior of the system. Then, the effect of changing the main parameters of the system on the harvested energy and vibration amplitude is investigated. Unlike other papers in this area of research, which only tend to maximize the output electrical power, both the vibratory response and output energy are investigated in this study. For this reason, a parameter, which is simply named Perfection Rate (PR), is defined. Finally, the effect of changing the load resistance and coupling coefficient on the PR parameter and system efficiency under the circumstances is investigated.

2.Mathematical Modeling

2-1. Coupled structure, piezoelectric, and wake oscillator model

A 2DOF model of the coupled structure and wake oscillator equipped with a piezoelectric device is schematically shown in part (A) of Figure (1). As indicated in this study, the piezoelectric device refers to the beam with a piezoelectric layer. In this figure, a cylinder of mass M_c and diameter D is subjected to the flow with uniform velocity U. Furthermore, $X(T)$ and $w(X_c,T)$ respectively show the in-line and cross-flow displacements. Also, X_c and Y_c represent in-line and cross-flow coordinates, respectively, and T denotes time. Moreover, L is the length of the piezoelectric device and t_p, t_b, K_x and C_x represent the piezoelectric thickness, beam thickness, stiffness, and damping of the device in in-line direction, respectively.

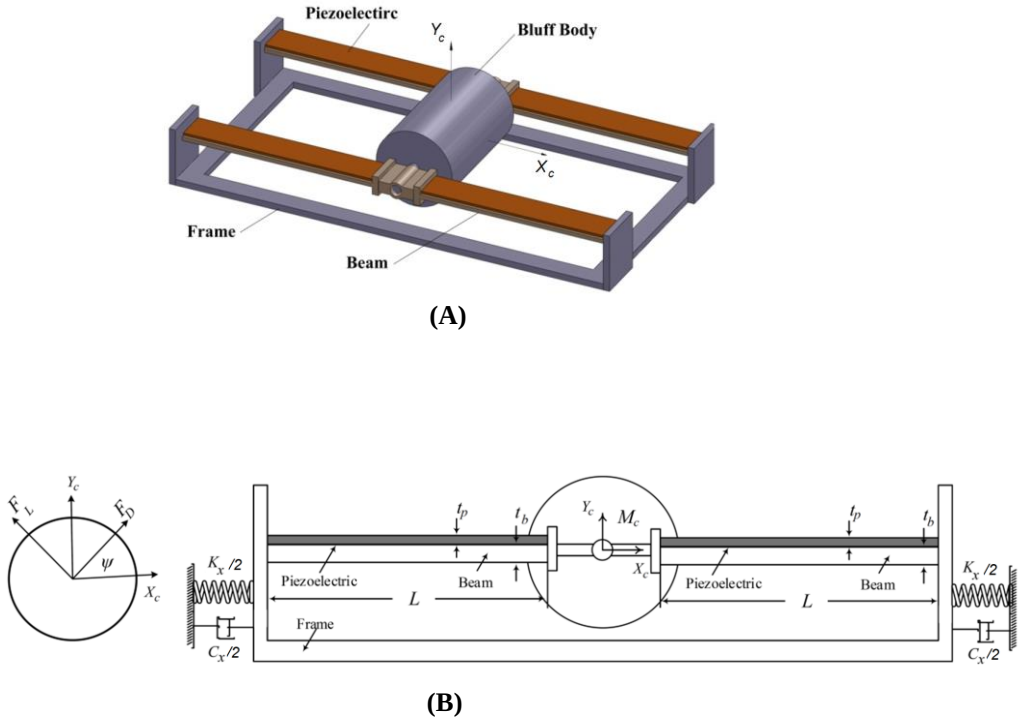

Fig1. 3D model of the energy harvester (A); cross section of the energy harvester (B)

To model the system, initially, the energy terms are derived and then they will be substituted in Lagrange equations to obtain the electromechanical equations of the system. The potential energy for the system, shown in Figure (1), is illustrated in the following form:

$$\pi = 2\int_{v_b} E_b \left(-Y_c \frac{\partial^2 w}{\partial X_c^2}\right)^2 dv_b + 2\int_{v_p} E_p \left\{\left(-Y_c \frac{\partial^2 w}{\partial X_c^2}\right)^2 + d_{31}\frac{V}{t_p}\left(-Y_c \frac{\partial^2 w}{\partial X_c^2}\right)\right\} dv_p + \frac{1}{2}K_x X^2 \tag{1}$$

where $w(X_c,T)$ and $V(T)$ are the transverse displacement of beam and electrical voltage, respectively. Also, d_{31}, E_p and E_b are piezoelectric strain constant and the Young's modulus of piezoelectric and beam, respectively. Note that the integrations are performed over the volume of the piezoelectric layer and beam and the subscripts p and b refer to piezoelectric patch and beam, respectively. Consequently, the volume of the piezoelectric and beam are presented as v_p and v_b. More details for deriving equation (1) are presented in Appendix A. The kinetic energy of the system is written as follows:

$$K = 2\int_{v_b} \rho_b \left(\frac{\partial w}{\partial T}\right)^2 dv_b + 2\int_{v_p} \rho_p \left(\frac{\partial w}{\partial T}\right)^2 dv_p + \frac{1}{2}M_c\left(\frac{\partial w}{\partial T}\bigg|_{X=L}\right)^2 + \frac{1}{2}M_t \dot{X}^2 \tag{2}$$

where ρ_b and ρ_p are the density of beam and piezoelectric, respectively; M_t is the total mass of the structure, and M_c is mass of the cylinder. More details for deriving equation (2) are written in Appendix B. The internal electrical energy can be calculated as follows [26]:

$$W_{ie} = -2\int_{v_p} \frac{V}{t_p}\left[\bar{e}_{31}\left(-Y_c \frac{\partial^2 w}{\partial X_c^2}\right) - e_{33}\frac{V}{t_p}\right] dv_p \tag{3}$$

In the above equation, $\bar{e}_{31}$ and e_{33} are effective piezoelectric stress constant and permittivity component at constant strain. The non-conservative virtual work of the system is given by:

$$\delta W_{nc} = \delta W_{nc}^{mech} + \delta W_{nc}^{elec} = F_y \delta w - F_x \delta X - C_x \dot{X}\ \delta X - 4\int_0^L c_a \frac{\partial w}{\partial T} dX_c\ \delta w - Q\delta V \tag{4}$$

in which c_a and Q are viscous damping coefficient and electric charge output. Note that, in the above equations, F_x and F_y respectively indicate fluid forces in the in-line and cross-flow directions. The transverse displacement of the beam can be given in the following form:

$$w(X_c, T) = \sum_{i=1}^{n} \varphi_i(X_c)\,.\,Y_i(T) \tag{5}$$

where $\varphi_i(X_c)$ and $Y_i(T)$ indicate the i^{th} mode shape and time response of the beam. Due to the fact that the first mode is the main mode, only the first vibration mode is considered in this study. Consequently, $\varphi(X_c)$ and $Y(T)$ are defined as mode shape and time response of the first vibration mode. The Lagrange equations are expressed as

$$\frac{d}{dt}\left(\frac{\partial K}{\partial \dot{X}_c}\right) - \frac{\partial K}{\partial X_c} + \frac{\partial \pi}{\partial X_c} - \frac{\partial W_{ie}}{\partial X_c} = F_x - C_x \dot{X} \tag{6}$$

$$\frac{d}{dt}\left(\frac{\partial K}{\partial \dot{Y}_c}\right) - \frac{\partial K}{\partial Y_c} + \frac{\partial \pi}{\partial Y_c} - \frac{\partial W_{ie}}{\partial Y_c} = -4\dot{Y}\int_0^L c_a \varphi^2\, dX_c + F_y \tag{7}$$

$$\frac{d}{dt}\left(\frac{\partial K}{\partial \dot{V}}\right) - \frac{\partial K}{\partial V} + \frac{\partial \pi}{\partial V} - \frac{\partial W_{ie}}{\partial V} = Q \tag{8}$$

Substituting equations (1) to (4) into the Lagrange equations and using the orthogonality conditions lead to finding the final equations of motion, which can be written as follows:

$$M_t\, \ddot{X} + C_x\, \dot{X} + K_x X = F_x \tag{9}$$

$$m_{eq}\ddot{Y} + c_{eq}\dot{Y} + k_{eq} Y - \theta V = F_y \tag{10}$$

$$2C_p \dot{V} + V/R + \theta \dot{Y} = 0 \tag{11}$$

In which Cp is the capacitance of piezoelectric layer, and other coefficients of the above equation are expressed as follows:

$$M_t = 4\left(\rho_b w_b t_b + \rho_p w_p t_p\right)L + M_c \tag{12}$$

$$m_{eq} = 4\left(\rho_b w_b t_b + \rho_p w_p t_p\right)\int_0^L \varphi^2\, dX_c + M_c\, \varphi^2\Big|_{X_c = L} \tag{13}$$

$$c_{eq} = 4c_a \int_0^L \varphi^2\, dX_c \tag{14}$$

$$k_{eq} = 4\left\{E_b I_b + E_p I_p\right\}\int_0^L (\varphi'')^2\, dX_c \tag{15}$$

$$\theta = 4\, w_p Y\left(E_p d_{31}\right)\int_0^L \varphi''\, dX_c \tag{16}$$

$$C_p = 2\, w_p L\, e_{33}/t_p \tag{17}$$

$$F_D = 0.5\rho D U^2 C_D \quad , \quad F_L = 0.5\rho D U^2 C_L \tag{18}$$

$$F_x = F_D\cos\psi + F_L\sin\psi \approx F_D + F_L\dot{Y}/U = 0.5\rho D U\left\{C_D U + C_L\dot{Y}\right\} \tag{19}$$

$$F_y = F_L\cos\psi + F_D\sin\psi \approx F_L - F_D\dot{Y}/U = 0.5\rho D U\left\{C_L U - C_D\dot{Y}\right\} \tag{20}$$

where C_D and C_L are the time-varying drag and lift coefficients, respectively. Furthermore, the boundary conditions are:

$$\phi(0) = 0 \quad , \quad \phi'(0) = 0 \quad , \quad EI\phi'''(L)q(t) = \frac{M_c}{4}\phi(L)\ddot{q}(t) \quad , \quad \phi'(L) = 0 \tag{21}$$

Moreover, the eigenfunction for the fixed-guided beam is given by the following equations, where λ is the eigenvalue of the first vibration mode. These equations are derived with the aid of reference [26].

$$\phi(X_c) = C\left\{\cos\left(\lambda X_c/L\right) - \cosh\left(\lambda X_c/L\right) + \sigma\left(\sin\left(\lambda X_c/L\right) - \sinh\left(\lambda X_c/L\right)\right)\right\} \tag{22}$$

$$\sigma = \frac{\left(\sin(\lambda) - \sinh(\lambda)\right) + \dfrac{M_c\lambda}{4\rho_t AL}\left(\cos(\lambda) - \cosh(\lambda)\right)}{\left(\cos(\lambda) + \cosh(\lambda)\right) - \dfrac{M_c\lambda}{4\rho_t AL}\left(\sin(\lambda) - \sinh(\lambda)\right)} \quad , \quad \left(\frac{\lambda}{L}\right)^4 = \frac{\rho A\omega^2}{EI} \tag{23}$$

Also, the orthogonality condition, which is shown as follows, can be used to find C.

$$\int_0^L \varphi^2(X_c)\rho A\, dX_c + \varphi^2(L)\frac{M_c}{4} = 1 \tag{24}$$

In the above equation, $\rho_t AL$ is the total mass of one beam and its attached piezoelectric. Based on the research done in the area of two-dimensional VIV, to improve the accuracy of modelling, several nonlinear terms should be added to the governing equations [18]. Therefore, the equations (9) and (10) can be re-written as follows:

$$(M_t + m_{fx})\ddot{X} + (C_x + C_{fx})\dot{X} + K_x(X + \alpha_x^* X^3 + \beta_x^* XY^2) = F_x \tag{25}$$

$$(m_{eq} + m_{fy})\ddot{Y} + (c_{eq} + C_{fy})\dot{Y} + k_{eq}(Y + \alpha_y^* Y^3 + \beta_y^* YX^2) - \theta V = F_y \tag{26}$$

The total effective mass of the cylinder is the sum of cylinder mass ($M_t \approx m_{eq}=m_s$) and fluid-added mass ($m_{fx}=m_{fy}=m_f=\rho C_M \pi D^2/4$), where ρ is the fluid density and C_M is the fluid-added mass coefficient. Note that C_M is assumed to be unity for the case of a circular cross section [12]. Furthermore, the total effective damping of the cylinder is equal to the sum of the hydrodynamic damping and structural damping (C_f+C_s), where the hydrodynamic damping is equal to ($C_{fx}=C_{fy}=C_f=\gamma(2\pi \mathrm{St} U/D)\rho D^2$) and the structural damping coefficients are considered to be equal in both X and Y directions ($C_x=c_{eq}=C_s$). Parameters γ and St in the presented relations are

respectively the stall parameter γ=0.8 [14] and the Strouhal number St=0.2 [12]. Moreover, α_x^*, α_y^*, β_y^* and β_y^* are the geometric coefficients that show the nonlinear behavior of the mass-spring structure and they are considered to be equal to 0.7 [27]. To describe the impact of vortices on the oscillating cylinder, two van der Pol equations have been presented in the following equations:

$$\ddot{p} + 2\varepsilon_x \omega_f (p^2 - 1)\dot{p} + 4\omega_f^2 p = S_x \tag{27}$$

$$\ddot{q} + \varepsilon_y \omega_f (q^2 - 1)\dot{q} + \omega_f^2 q = S_y \tag{28}$$

where p and q are reduced vortex drag and lift coefficients (p=2C_D/C_{D0}, q=2CL/C_{L0}) [27]. Furthermore, C_{D0} and C_{L0} are drag and lift coefficients of a stationary cylinder and are respectively taken as 0.2 [28] and 0.3 [12]. Herein, the effect of two-dimensional cylinder fluctuations on the surrounding vortices are simulated as the excitation terms (S_x=$\Lambda_x\ddot{X}/D$ and S_y=$\Lambda_y\ddot{Y}/D$). In this study, the so-called wake–cylinder coupling coefficients (Λ_x, Λ_y), based on the previous experimental studies, are considered as Λ_x=Λ_y=12 [14]. Moreover, ε_x and ε_y are experimental wake coefficients and they are respectively equal to 0.3 and $0.00234e^{0.228m^*}$, in which mass ratio m^* is equal to 1.4 [14, 18]. In addition, the vortex-shedding angular frequency is obtained using the relation ω_f=2πStU/D [12]. Consider that the initial conditions are p=q=2 and velocities are zero. Therefore, in the case of S_x=S_y=0 and ε_x>0, ε_y≤1, van der Pol equations settle a stable quasi-harmonic oscillation around p_0=q_0=2 at the angular frequency ω_f [29]. Note that equations (25) to (28) and (11) are coupled equations, which describe the electromechanical behavior of the system.

2-2. Normalized equations

Defining dimensionless variables for in-line displacement x=X/D, cross-flow displacement y=Y/D, generated voltage v=V/v_0, and time t=$\omega_{ny}T$ leads to find the normalized form of the electromechanical equations. The coupled electromechanical equations are written as follows:

$$\ddot{x} + \lambda_x \dot{x} + f^{*2}(x + \alpha_x x^3 + \beta_x x y^2) = M_D \Omega^2 p + 2\pi M_L \Omega^2 (q\dot{y}/U_r) \tag{29}$$

$$\ddot{y} + \lambda_y \dot{y} + y + \alpha_y y^3 + \beta_y y x^2 - (v/4\pi^2) = M_L \Omega^2 q - 2\pi M_D \Omega^2 (p\dot{y}/U_r) \tag{30}$$

$$\ddot{p} + 2\varepsilon_x \Omega (p^2 - 1)\dot{p} + 4\Omega^2 p = \Lambda_x \ddot{x} \tag{31}$$

$$\ddot{q} + \varepsilon_y \Omega (q^2 - 1)\dot{q} + \Omega^2 q = \Lambda_y \ddot{y} \tag{32}$$

$$\dot{v} + \left(RC_P \omega_{ny}\right)^{-1} v + 4\pi^2 \theta^2 \left(C_P (m_{eq} + m_{fy})\omega_{ny}^2\right)^{-1} \dot{y} = 0 \tag{33}$$

where α_y=$\alpha_y^* D^2$ and β_y=$\beta_y^* D^2$ are the geometrically nonlinear coefficients [18], and combined fluid-structural damping terms λ_x and λ_y, are given by:

$$\lambda_x = 2\xi_x f^* + (\gamma\Omega/\mu_x) \quad , \quad \lambda_y = 2\xi_y + (\gamma\Omega/\mu_y) \tag{34}$$

where f*=fnx/fny and Ω=ωf/ωny=StUr are frequency ratios [14, 18] and μx and μy are mass ratios:

$$\mu_x = \frac{M_t + m_{fx}}{\rho D^2} \quad , \quad \mu_y = \frac{m_{eq} + m_{fy}}{\rho D^2} \tag{35}$$

Also, ξ_x and ξ_y are structural damping coefficients, which are written as follows:

$$\xi_x = \frac{C_x}{2(M_t + m_{fx})\omega_{nx}} \quad , \quad \xi_y = \frac{c_{eq}}{2(m_{eq} + m_{fy})\omega_{ny}} \tag{36}$$

Furthermore, structural natural frequencies in still water are given by [18]:

$$\omega_{nx} = \sqrt{K_x/(M_t + m_{fx})} \quad , \quad \omega_{ny} = \sqrt{k_{eq}/(m_{eq} + m_{fy})} \tag{37}$$

The reduced form of flow velocity is given by Ur=2πU/(ωnyD) [13]. For normalizing the displacement equations, two parameters for stream-wise and transverse mass parameters are as follows [18]:

$$M_D = \frac{C_{D0}}{2}\frac{1}{8\pi^2 St^2 \mu_x} \quad , \quad M_L = \frac{C_{L0}}{2}\frac{1}{8\pi^2 St^2 \mu_y} \tag{38}$$

Furthermore, the dimensionless form of the generated voltage $v=V/v_0$ is given by:

$$v_0 = \left(\rho D^3 L_c \mu_y f_{ny}^2\right)/\theta \tag{39}$$

where L_c is the circular cylinder length.

3.Results and Discussion

3-1. Case study

The material and geometric properties of the coupled structure and wake oscillator system are listed in Table (1). Notice that these properties are as same as the previous experimental studies. Note that this experiment is done in the uniform steady flow with Reynolds numbers between 2×10^3 and 5×10^4. Therefore, the fluid flow is in sub-critical range of Reynolds number [18].

Table1. Properties of the coupled structure of cylinder and wake

Physical parameters	Values	Physical parameters	Values
D (m)	0.114	ξ_x	0.047
f_{nx} (Hz)	0.316	ξ_y	0.01
f_{ny} (Hz)	0.312	μ_y	0.6π
ρ (kg/m^3)	1000	L_c (m)	1.037

To validate the results, amplitudes of the cross-flow and in-line vibrations of the cylindrical bluff body (without the energy harvesting device) are compared with the previous experimental results. Figure (2) shows the comparison of theoretical modeling with the experimental results for cross-flow and in-line oscillations [17, 18]. According to this figure, the following results are mentioned.

1. 1.In the synchronization regime ($4<U_r<12$), the cylinder oscillations in the cross-flow direction is more than the in-line oscillations.
2. 2.Although numerical responses and experimental responses in the in-line direction have more discrepancies, these results in the cross-flow direction can confirm the lock-in region and maximum amplitude adequately.

Consequently, the cross-flow simulation is more reliable and proper for energy harvesting. Therefore, in the present study, the piezoelectric device is attached to the beam, which is used to act in the cross-flow direction.

It is worth mentioning that, in this study, only the first vibration mode is considered because:

1. It is more typical to use piezoelectric energy harvesting systems only for the first vibration mode.
2. By considering more vibration modes, the number of fluid-structure interaction relations will be more than 4 coupled equations and it is much harder to match the numerical simulation with experimental responses.

Therefore, it is possible to improve the experimental and numerical responses by considering more mode shapes but, this suggestion needs more complicated investigations.

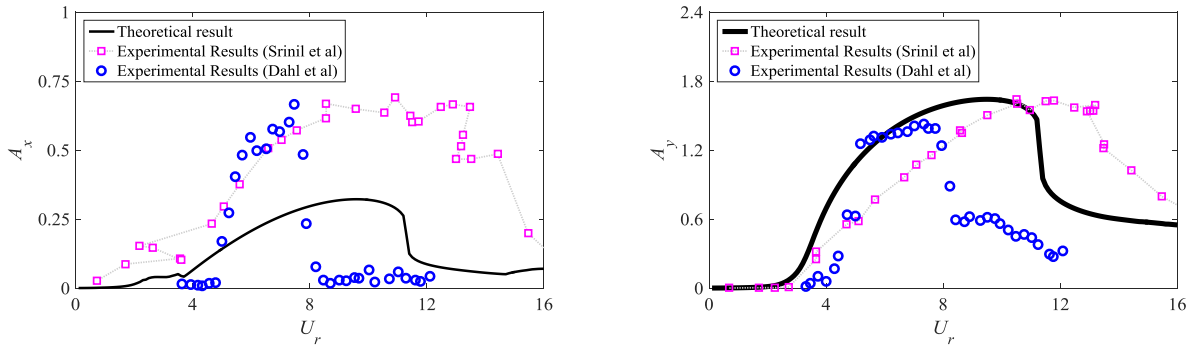

(A) **(B)**

Fig.2. Comparisons of in-line (A) and cross-flow amplitudes (B) with the experimental data [17, 18]

3-2. Effect of changing the main parameters on the generated power

Properties of the piezoelectric layer attached to the VIV-powered energy harvesting system are shown in Table (2).

Table2. Properties of the piezoelectric device [30]

Physical parameters	Values	Physical parameters	Values
C_P (nF)	120	θ (mN/V)	1.55

Response of the system undergoing VIV, which is equipped with the piezoelectric device, is shown in Figure (3). For better presentation, the time response of the vibratory system in several reduced velocities (U_r=4, 10, and 16) are shown in this figure. As expected, the highest vibration

amplitudes are shown in the lock-in range. In the next subsections, the influence of varying different parameters on the dynamic behavior of the presented system is investigated.

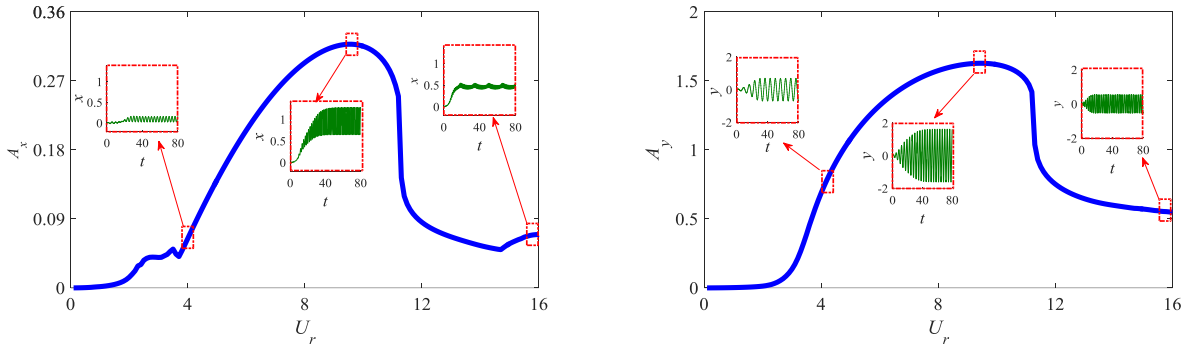

(A) **(B)**

Fig.3. Amplitude responses of the in-line (A); and cross-flow vibrations (B) of the cylinder with the piezoelectric device (R=100KΩ)

3-2-1. effect of changing load resistance on the generated power

As shown in Figure (4), increasing the load resistance leads to a decrease in the amplitudes of in-line and cross-flow vibrations. The reason for this behavior lies in the fact that raising the load resistance leads to an increase in the harvested electrical energy, and consequently, it leads to reducing the mechanical energy.

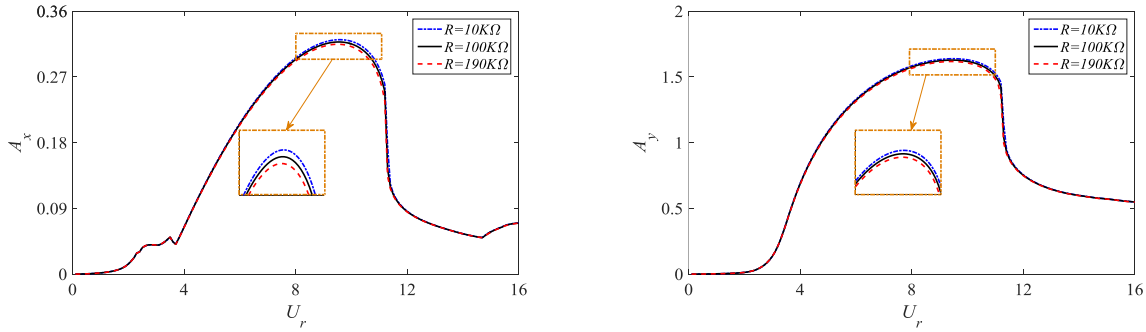

(A) **(B)**

Fig.4. Variations of the in-line (A) and cross-flow amplitudes (B) for different load resistances

3-2-2. effect of changing electromechanical coupling coefficient on the generated power

The significant effect of changing the load resistance on the RMS of the harvested power is shown in part (A) of Figure (5). As shown in this figure, the maximum power can be harvested under the synchronization regime. Note that the RMS value gives a measure of the average energy in the signal. The RMS of the harvested power is calculated as follows:

$$P_{RMS} = \left\{ \frac{1}{N} \sum_{i=1}^{N} \left(v_{(t_i)}^2 / R \right)^2 \right\}^{1/2} \tag{40}$$

where N is the signal length and t_i is the i^{th} element of the time vector. Effect changing the load resistance on RMS of the harvested power, in several values of the reduced velocity, is shown in part (B) of Figure (5). The power in this figure is depicted versus the load resistance, which is increased up to 190kΩ.

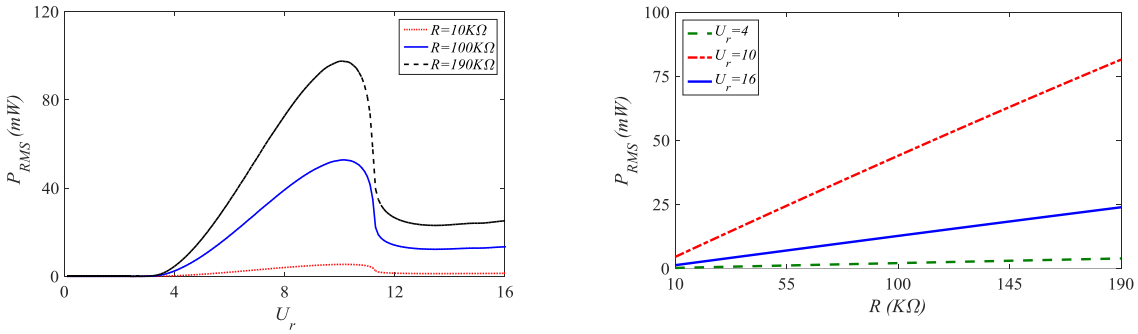

(A) **(B)**

Fig.5. Variations of harvested power versus the reduced velocity (A) and the load resistance (B)

Note that the electromechanical coupling coefficient can be written as [31]:

$$\theta = \left\{\left(\omega_{\mathrm{n,oc}}^2 - \omega_{\mathrm{n,sc}}^2\right) M_{\mathrm{eff}} C_{\mathrm{p}}\right\}^{1/2} \tag{41}$$

where $\omega_{n,oc}$ and $\omega_{n,sc}$ are respectively the open circuit and short circuit natural frequencies of the energy harvesting system, which can experimentally be obtained and C_P is the total capacitance of the piezoelectric device, which is related to the dimension and dielectric constant of the piezoelectric device. Therefore, the electromechanical coupling coefficient can be variable due to system properties. To change this parameter in real physical system, different methods are suggested. For instance, one way to increase the electromechanical coupling coefficient is to increase its capacitance. Another effective method is modifying the effective length of the piezoelectric layer by varying the distance between two points of electrodes. Furthermore, changing other parameters like the thickness of the piezoelectric layer and electric field component is effective on this parameter [32-34].

Herein this question may be posed:"what is the effect of varying electromechanical coupling coefficient on vibratory and energy behavior of the presented system?" The effect of changing the electromechanical coupling coefficient on the in-line and cross-flow amplitudes of the discussed system in different reduced velocities is shown in Figure (6). As shown in this figure, increasing electromechanical coupling coefficient leads to a decrease in the amplitude of in-line and cross-flow vibrations.

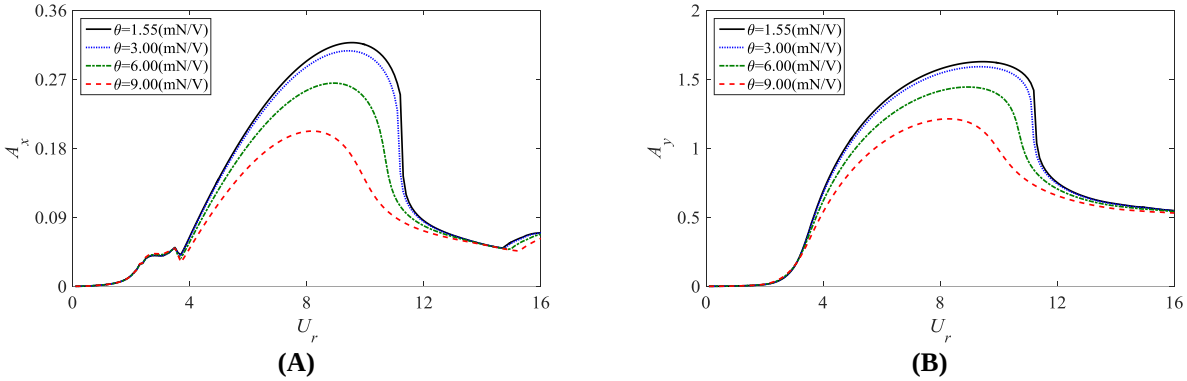

Fig.6. Variations of the in-line (A) cross-flow (B) amplitudes versus the reduced velocity with variable electromechanical coupling coefficient (R=100KΩ)

3-2-3. effect of changing electromechanical coupling coefficient and load resistance on the generated power

The effect of changing both load resistance and electromechanical coupling coefficient is shown in Figure (7). Regarding this figure, it can be concluded that increasing both the electromechanical coupling coefficient and load resistance leads to increasing the harvested power, and as expected, the system generates more power in the synchronization range.

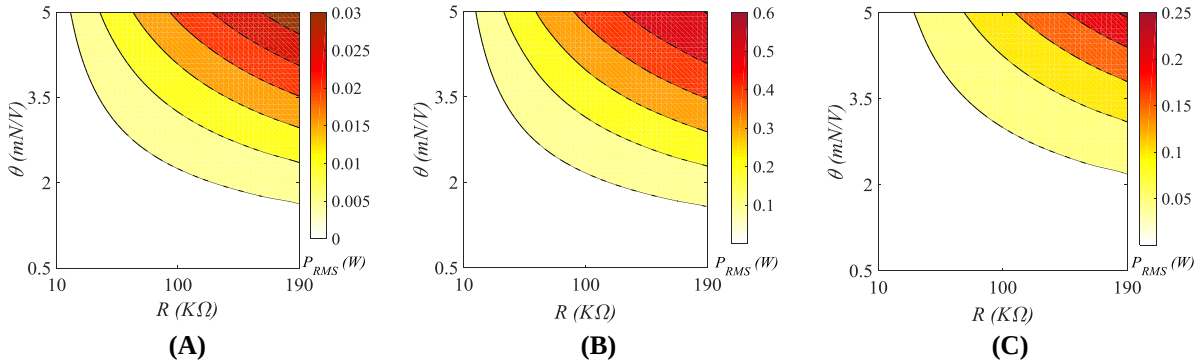

Fig.7. Variations of the RMS power versus the load resistance and the electromechanical coupling coefficient in the pre-synchronization regime for U_r=4 (A), synchronization regime for U_r=10 (B), and post-synchronization regime for U_r=16 (C)

Inspecting the figures, the following conclusions are found out:

1. Regarding part (B) of Figure (4), in high reduced velocity (U_r=16), the vibration amplitude is more than three times smaller than the highest vibration amplitude in the synchronization regime (U_r=10). Furthermore, according to Figure (7), the RMS value of the harvested power in the synchronization regime can be 2.4 times larger than the harvested power in the post-synchronization regime. In other words, RMS value of generated power does not linearly increase with the growth of vibration amplitudes.
2. According to the fact that the system oscillations are higher in the lock-in range, the vortex-induced vibration-based energy harvesters should be used near their fundamental frequency. Moreover, it is worth mentioning that the large deflection of the beam and piezoelectric transducer may lead to structural failure.

Regarding these aspects, the system should be designed to generate maximum power with less damage. Therefore, maximizing the harvested energy (electrical-based modelling) and minimizing the mechanical deflection (mechanical-based modelling) should simultaneously be considered. The so-called Perfection Rate (*PR*), which summarizes both electrical-based and mechanical-based modellings in a parameter, is defined as follows:

$$\text{PR }(\%) = 100 \times \left\{ WF\left(P_{RMS}/P_{\max}\right) + \left(1-WF\right)\left(1-A_y/A_{\max}\right) \right\} \tag{42}$$

in which *WF* is the weighting factor for the energy-based modelling. Inspecting this equation, raising *WF* leads to an increase in electrical energy importance and a decrease in mechanical energy importance in the system. It is also noted that by reduction of mechanical energy importance, the effect of changing vibration amplitudes on the system and subsequently the probability of system failure decreases. Variation of the *PR* parameter with the load resistance and electromechanical coupling coefficient is depicted in Figure (8). As shown in this figure, when the importance of the electrical energy is less (*WF*=0.3), for all the values of load resistance and electromechanical coupling coefficient, the energy harvester's efficiency is more in the post-synchronization range (U_r=16).

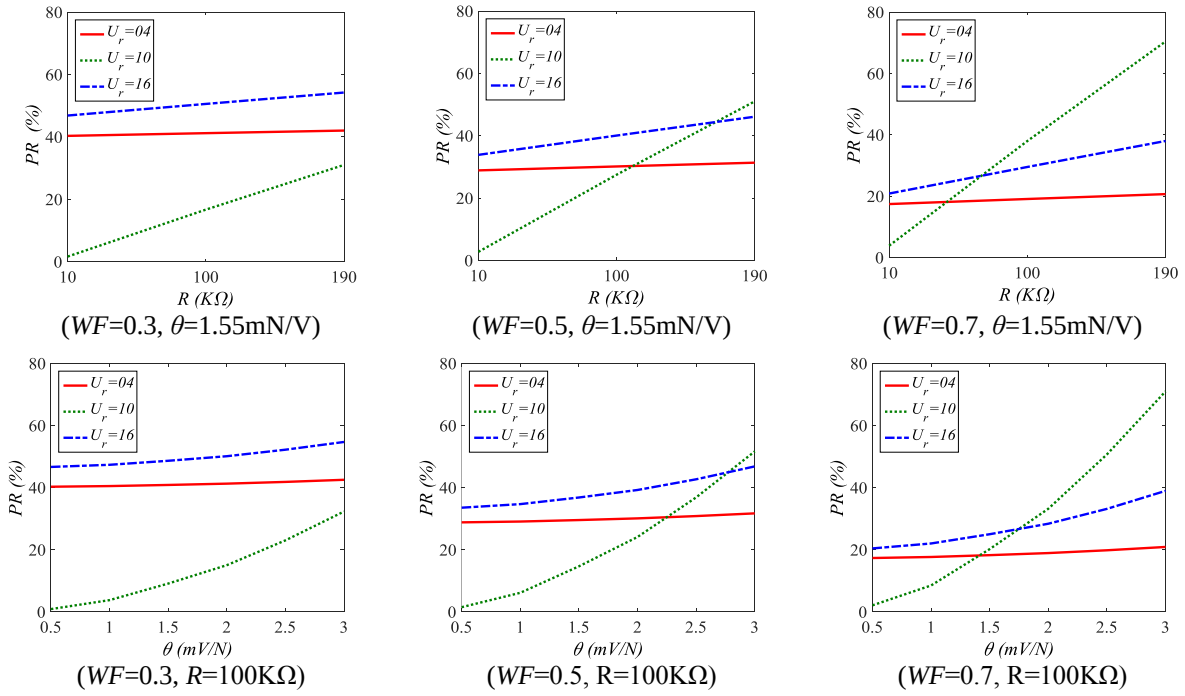

(*WF*=0.3, θ=1.55mN/V) (*WF*=0.5, θ=1.55mN/V) (*WF*=0.7, θ=1.55mN/V)

(*WF*=0.3, *R*=100KΩ) (*WF*=0.5, R=100KΩ) (*WF*=0.7, R=100KΩ)

Fig.8. Variations of the perfection rate in pre-synchronization, synchronization, and post-synchronization regimes versus load resistance (θ=1.55mN/V)

Moreover, when the importance of the electrical-based and mechanical-based modelling is the same (*WF*=0.5), for a wide range of load resistance and electromechanical coupling coefficient values, the VIV-based energy harvester works better in post-synchronization regime (U_r=16). Also, for load resistance values of more than 170 KΩ and electromechanical coupling coefficient values of more than 2.8 mN/V, the energy harvester is advantageous in the lock-in range

(U_r=10). The energy harvester's behavior is similar when the importance of the electrical-based modelling is more (*WF*=0.7), and the system is efficient for the load resistance up to 70 KΩ and electromechanical coupling coefficient up to 1.8 mN/V in the synchronization range (U_r=10).

Therefore, the following results are derived:

1. By increasing electrical energy importance (increasing *WF*), the system performance improves in the lock-in range for high values of load resistance and electromechanical coupling coefficient.
2. By increasing mechanical energy importance (decreasing *WF*), the system efficiency enhances in the post-synchronization range and for low values of load resistance and electromechanical coupling coefficient.

Therefore, it is possible to design a system based on values of load resistance, electromechanical coupling coefficient, *WF*, and U_r. Also, in the lock-in range (U_r=10) the *PR* is maximum for high values of load resistance and electromechanical coupling coefficient (*PR*=70%).

It is worth adding that the piezoelectric materials have a higher power density compared to other energy harvesting methods. In this study, the maximum of the harvested electrical power, from four piezoelectric devices with dimensions 30×5×0.15 mm, is equal to 0.6 W. Therefore, the power density, which is calculated by dividing the output power by the volume of energy harvester [26], is equal to 6.67 W/cm^3.

4.Conclusion

In this paper, the vortex-induced vibration of a circular cylinder, which is connected to a piezoelectric energy harvester, has been studied. First, governing equations of motion has been derived and the influence of variable parameters of the dynamic behavior of the system has been investigated so as to enhance the system's efficiency. As a result, it was denoted that increasing each of the load resistance or electromechanical coupling coefficient can lead to decreasing vibration amplitudes. Also, results illustrate that the highest power can be harvested in the lock-in range. Furthermore, regarding high mechanical stress in the lock-in range, energy harvesting in the post-synchronization range (U_r>12) is safer. Also, regarding the *PR* parameter, when *WF*=0.5, it is concluded that the systems with load resistances of less than 170KΩ should work in the post-synchronization regime. Moreover, it was demonstrated that in the case of systems with small electromechanical coupling coefficients, like small piezoelectric devices, energy harvesting in the post-synchronization regime is preferred.

Appendix A

To calculate the potential energy of the piezoelectric patch and beam, the first step is to define the strain of σ and stress of ε as [26]

$$\varepsilon = -Y_c \frac{\partial^2 w}{\partial X_c^2} \quad , \quad \sigma_b = E_b \varepsilon \quad , \quad \sigma_p = E_p \varepsilon + E_p d_{31} E_3 \quad , \quad E_3 = \frac{V}{t_p} \tag{A1}$$

where E_3 is the electric field component in the cross-flow direction of Y_c. Also, the potential energy of each piezoelectric and beam can be calculated as

$$\pi_1 = \frac{1}{2}\int_{v_b} \sigma_b \varepsilon \, dv_b + \frac{1}{2}\int_{v_p} \sigma_p \varepsilon \, dv_p \tag{A2}$$

In the second step, by substituting stress and strain relations of (A1) into the potential energy relation of (A2), the ultimate form of the potential energy of each piezoelectric patch and beam is given by

$$\pi_1 = \frac{1}{2}\int_{v_b} E_b \left(-Y_c \frac{\partial^2 w}{\partial X_c^2}\right)^2 dv_b + \frac{1}{2}\int_{v_p} E_p \left\{\left(-Y_c \frac{\partial^2 w}{\partial X_c^2}\right)^2 + d_{31}\frac{V}{t_p}\left(-Y_c \frac{\partial^2 w}{\partial X_c^2}\right)\right\} dv_p \tag{A3}$$

Moreover, the potential energy of the spring in in-line direction is

$$\pi_2 = \frac{1}{2} K_x X^2 \tag{A4}$$

Finally, the total potential energy of the structure is obtained by adding the potential energy of (A4) to the potential energy of 4 piezoelectric patches and beams in (A3).

$$\pi = 2\int_{v_b} E_b \left(-Y_c \frac{\partial^2 w}{\partial X_c^2}\right)^2 dv_b + 2\int_{v_p} E_p \left\{\left(-Y_c \frac{\partial^2 w}{\partial X_c^2}\right)^2 + d_{31}\frac{V}{t_p}\left(-Y_c \frac{\partial^2 w}{\partial X_c^2}\right)\right\} dv_p + \frac{1}{2} K_x X^2 \tag{A5}$$

Appendix B

To derive the kinetic energy of the structure, first, the kinetic energy of each piezoelectric patch and beam in cross-flow direction is calculated as

$$K_1 = \frac{1}{2}\int_{v_b} \rho_b \left(\frac{\partial w}{\partial T}\right)^2 dv_b + \frac{1}{2}\int_{v_p} \rho_p \left(\frac{\partial w}{\partial T}\right)^2 dv_p \tag{B1}$$

Moreover, the kinetic energy of the cylinder in cross-flow direction is given by

$$K_2 = \frac{1}{2} M_c \left(\left.\frac{\partial w}{\partial T}\right|_{X=L}\right)^2 \tag{B2}$$

Similarly, the total kinetic energy of the structure in in-line direction is

$$K_3 = \frac{1}{2} M_t \dot{X}^2 \quad , \quad M_t = 4\left(\rho_b w_b t_b + \rho_p w_p t_p\right) L + M_c \tag{B3}$$

where M_t is the total mass of the structure. Finally, by adding the kinetic energy of 4 piezoelectric patches and beams in equation (B1) to (B2) and (B3), the total kinetic energy of the structure in both in-line and cross-flow directions is obtained as

$$K = 2\int_{v_b} \rho_b \left(\frac{\partial w}{\partial T}\right)^2 dv_b + 2\int_{v_p} \rho_p \left(\frac{\partial w}{\partial T}\right)^2 dv_p + \frac{1}{2} M_c \left(\left.\frac{\partial w}{\partial T}\right|_{X=L}\right)^2 + \frac{1}{2} M_t \dot{X}^2 \tag{B4}$$

References

[1] S.-C. Huang, C.-Y. Tsai, Theoretical analysis of a new adjustable broadband PZT beam vibration energy harvester, International Journal of Mechanical Sciences, 105 (2016) 304-314.
[2] M. Karimi, A.H. Karimi, R. Tikani, S. Ziaei-Rad, Experimental and theoretical investigations on piezoelectric-based energy harvesting from bridge vibrations under travelling vehicles, International Journal of Mechanical Sciences, 119 (2016) 1-11.
[3] Z. Yang, Y. Tan, J. Zu, A Multi-impact Frequency Up-converted Magnetostrictive Transducer for Harvesting Energy from Finger Tapping, International Journal of Mechanical Sciences, (2017).
[4] D.P. Arnold, Review of Microscale Magnetic Power Generation, IEEE Transactions on Magnetics, 43 (2007) 3940-3951.
[5] P.D. Mitcheson, P. Miao, B.H. Stark, E. Yeatman, A. Holmes, T. Green, MEMS electrostatic micropower generator for low frequency operation, Sensors and Actuators A: Physical, 115 (2004) 523-529.
[6] S.R. Anton, H.A. Sodano, A review of power harvesting using piezoelectric materials (2003–2006), Smart materials and Structures, 16 (2007) R1.
[7] K. Cook-Chennault, N. Thambi, A. Sastry, Powering MEMS portable devices—a review of non-regenerative and regenerative power supply systems with special emphasis on piezoelectric energy harvesting systems, Smart Materials and Structures, 17 (2008) 043001.
[8] A. Afsharfard, A. Farshidianfar, Application of single unit impact dampers to harvest energy and suppress vibrations, Journal of Intelligent Material Systems and Structures, (2014) 1045389X14535012.
[9] A. Abdelkefi, Aeroelastic energy harvesting: A review, International Journal of Engineering Science, 100 (2016) 112-135.
[10] A. Postnikov, E. Pavlovskaia, M. Wiercigroch, 2DOF CFD calibrated wake oscillator model to investigate vortex-induced vibrations, International Journal of Mechanical Sciences.
[11] R.E.D. Bishop, A.Y. Hassan, The Lift and Drag Forces on a Circular Cylinder Oscillating in a Flowing Fluid, Proceedings of the Royal Society of London. Series A. Mathematical and Physical Sciences, 277 (1964) 51-75.
[12] R.D. Blevins, Flow-induced vibration, (1990).
[13] T. Sarpkaya, A critical review of the intrinsic nature of vortex-induced vibrations, Journal of fluids and structures, 19 (2004) 389-447.
[14] M.L. Facchinetti, E. De Langre, F. Biolley, Coupling of structure and wake oscillators in vortex-induced vibrations, Journal of Fluids and structures, 19 (2004) 123-140.
[15] A. Farshidianfar, H. Zanganeh, A modified wake oscillator model for vortex-induced vibration of circular cylinders for a wide range of mass-damping ratio, Journal of Fluids and Structures, 26 (2010) 430-441.
[16] N. Jauvtis, C. Williamson, The effect of two degrees of freedom on vortex-induced vibration at low mass and damping, Journal of Fluid Mechanics, 509 (2004) 23-62.
[17] J. Dahl, F. Hover, M. Triantafyllou, Two-degree-of-freedom vortex-induced vibrations using a force assisted apparatus, Journal of Fluids and Structures, 22 (2006) 807-818.
[18] N. Srinil, H. Zanganeh, A. Day, Two-degree-of-freedom VIV of circular cylinder with variable natural frequency ratio: Experimental and numerical investigations, Ocean Engineering, 73 (2013) 179-194.
[19] A. Abdelkefi, A. Nayfeh, M. Hajj, Enhancement of power harvesting from piezoaeroelastic systems, Nonlinear Dynamics, 68 (2012) 531-541.
[20] A. Abdelkefi, M. Hajj, A. Nayfeh, Phenomena and modeling of piezoelectric energy harvesting from freely oscillating cylinders, Nonlinear Dynamics, 70 (2012) 1377-1388.
[21] A. Abdelkefi, M.R. Hajj, A.H. Nayfeh, Power harvesting from transverse galloping of square cylinder, Nonlinear Dynamics, 70 (2012) 1355-1363.
[22] J.J. Allen, A.J. Smits, ENERGY HARVESTING EEL, Journal of Fluids and Structures, 15 (2001) 629-640.
[23] S. Pobering, N. Schwesinger, A novel hydropower harvesting device, in: MEMS, NANO and Smart Systems, 2004. ICMENS 2004. Proceedings. 2004 International Conference on, IEEE, 2004, pp. 480-485.
[24] H.D. Akaydin, N. Elvin, Y. Andreopoulos, Energy harvesting from highly unsteady fluid flows using piezoelectric materials, Journal of Intelligent Material Systems and Structures, 21 (2010) 1263-1278.
[25] J. Xie, J. Yang, H. Hu, Y. Hu, X. Chen, A piezoelectric energy harvester based on flow-induced flexural vibration of a circular cylinder, Journal of Intelligent Material Systems and Structures, 23 (2012) 135-139.
[26] A. Erturk, D.J. Inman, Piezoelectric energy harvesting, John Wiley & Sons, 2011.
[27] N. Srinil, H. Zanganeh, Modelling of coupled cross-flow/in-line vortex-induced vibrations using double Duffing and van der Pol oscillators, Ocean Engineering, 53 (2012) 83-97.

[28] I. Currie, D. Turnbull, Streamwise oscillations of cylinders near the critical Reynolds number, Journal of Fluids and Structures, 1 (1987) 185-196.
[29] A.H. Nayfeh, Introduction to Perturbation Techniques, Wiley, 1993.
[30] A. Mehmood, A. Abdelkefi, M. Hajj, A. Nayfeh, I. Akhtar, A. Nuhait, Piezoelectric energy harvesting from vortex-induced vibrations of circular cylinder, Journal of Sound and Vibration, 332 (2013) 4656-4667.
[31] L. Zhao, L. Tang, Y. Yang, Comparison of modeling methods and parametric study for a piezoelectric wind energy harvester, Smart materials and Structures, 22 (2013) 125003.
[32] S. Kim, W.W. Clark, Q.-M. Wang, Piezoelectric energy harvesting with a clamped circular plate: analysis, Journal of intelligent material systems and structures, 16 (2005) 847-854.
[33] S. Kim, W.W. Clark, Q.-M. Wang, Piezoelectric energy harvesting with a clamped circular plate: experimental study, Journal of Intelligent Material Systems and Structures, 16 (2005) 855-863.
[34] D.L. DeVoe, Piezoelectric thin film micromechanical beam resonators, Sensors and Actuators A: Physical, 88 (2001) 263-272.